Available online at www.sciencedirect.com
ScienceDirect
Trans. Nonferrous Met. Soc. China 31(2021) 382−390
Transactions of Nonferrous Metals Society of China
www.tnmsc.cn

# Basal stacking fault induced twin boundary gliding, twinning disconnection and twin growth in hcp Ti from the first-principles

Qi QIAN[1*], Zheng-qing LIU[1*], Yong JIANG[1,2], Yi-ren WANG[1], Xing-long AN[2], Min SONG[2]

1. School of Materials Science and Engineering, Central South University, Changsha 410083, China;
2. State Key Laboratory of Powder Metallurgy, Central South University, Changsha 410083, China

Received 16 March 2020; accepted 6 September 2020

**Abstract:** First-principles calculations were performed to investigate the structures and energetics of $\{10\bar{1}n\}$ coherent twin boundaries (CTBs) and glide twin boundaries (GTBs) in hexagonal close-packed (hcp) Ti. The formation mechanism of GTBs and their correlation with twin growth were fundamentally explored. Results suggested that GTBs can form from the gliding of CTBs, through their interaction with basal stacking fault. The gliding eventually restored the CTB structures by forming a pair of single-layer twinning disconnections. The pile-up of twinning disconnections should be responsible for the wide steps at twin boundaries as observed in high-resolution transmission electron microscopy, which can further promote twin growth. Possible effects of various alloying elements on pinning twin boundaries were also evaluated, to guide the strengthening design of Ti alloys.

**Key words:** twin boundary; stacking fault; twinning disconnection; twin growth; first principles

## 1 Introduction

Twins are prone to form in crystals with low or medium stacking-fault energies [1], usually through the nucleation of faulted layers during the solidification [2], vapor deposition [3], or annealing recrystallization [4]. When crystal formability suffers seriously from a lack of independent slip systems (such as in plastically deformed hcp metals), or from the sharply increased stress of dislocation slip especially at low temperatures (such as in impact-loaded fcc-Cu [5] and bcc-Fe [6]), deformation twinning can also be induced. Deformation twins can even turn the unfavourably oriented grains to a more favourable slip orientation [7]. Typical twinning modes in the hcp crystals are $\{10\bar{1}1\}\langle 10\bar{1}2\rangle$, $\{10\bar{1}2\}\langle 10\bar{1}1\rangle$, $\{11\bar{2}1\}\langle 11\bar{2}6\rangle$ and $\{11\bar{2}2\}\langle 11\bar{2}3\rangle$ [7,8]. The formation of twins has been generally believed to be closely related to partial dislocations and twinning disconnections (TDs) on non-basal twinning planes [7,9−12]. For instance, $\{10\bar{1}2\}$ twins can nucleate from the simultaneous nucleation of multiple TDs, or perhaps more energetically favourably, from the simultaneous nucleation of non-basal partial dislocations and multiple TDs [12]. Such TDs can nucleate from non-planar dissociations of *a*, *a*+*c*, or *c* dislocations [13−16]. The twin can grow as TDs glide at the $\{10\bar{1}2\}$ twin boundary. The core structure and high mobility of TDs have been identified by high-resolution transmission electron microscopy (HRTEM) [17,18]. Other mechanisms based on atomic shuffling and zonal dislocations also exist [19,20], but still have many details in debates.

Coherent twin boundary (CTB) is the simplest structural version of twin boundaries (TBs), where the twin lattice is exactly a mirror reflection of the parent lattice [7,21]. Considerable theoretical

**Corresponding author:** Yong JIANG, E-mail: yjiang@csu.edu.cn; Min SONG, E-mail: msong@csu.edu.cn
*Qi QIAN and Zheng-qing LIU contributed equally to this work
DOI: 10.1016/S1003-6326(21)65503-6

efforts have been devoted to the structures and energetics of $\{10\bar{1}n\}$ and $\{11\bar{2}n\}$ CTBs in hcp Mg, Zr, and Ti, using various numerical methods including molecular statics (MS) [22], molecular dynamics (MD) [23], and first-principles density functional theory (DFT) [21,24,25]. Another major form of TBs is the glide twin boundary (GTB). The concept of GTB was firstly proposed for $\{10\bar{1}2\}\langle 10\bar{1}1\rangle$ twins [26], where GTBs were modeled by shifting one side lattice of CTB against the other along $\langle 10\bar{1}1\rangle$ on the twinning plane of $\{10\bar{1}2\}$. Soon later, $\{10\bar{1}2\}$ GTBs were observed by HRTEM characterizations in hcp Zn, and energetics calculations suggested that the GTBs could be preferred to forming under non-equilibrium conditions [27]. Recently, energetics calculations have been further extended to the $\{10\bar{1}2\}$ GTBs in hcp Mg and Au, as well as the $\{10\bar{1}1\}$ GTBs in hcp Mg and Au [28−31]. These GTBs were all predicted as high energy and metastable, as compared to their CTB counterparts, and their formation mechanism remains unclear.

Basal dislocations can induce basal stacking faults (SFs) during deformation [32]. However, in contrast to a number of studies on non-basal partial dislocations, the roles of basal partial dislocations (and basal SFs) in twin growth are rarely studied. Very recently, the connection between basal SFs and twins has been experimentally suggested, based on the high-density presence of basal SFs inside $\{10\bar{1}2\}\langle 10\bar{1}1\rangle$ deformation twins under HRTEM [33]. Besides, profuse $I_1$ SFs (defined as in hcp systems by removing one basal layer followed by a slip of $1/3\langle 01\bar{1}0\rangle$) induced by basal dislocations were observed closely accompanying the growth of $\{10\bar{1}2\}$ twins in pure Mg using in-situ tension experiments under transmission electron microscopy (TEM) [34]. MD simulations [35,36] also suggested that the intersection of one $I_1$ SF with a $\{10\bar{1}1\}$ TB could emit a single-layer TD, which cannot glide along the TB but move by climbing to facilitate the development of twin embryos [35]. No first-principles efforts have been made to explore the complex interplays among basal SFs, TB gliding, TDs, and further twin growth, especially for both CTBs and GTBs in hcp systems.

In this work, we take hcp Ti as an exemplary system and investigate the structures and energetics of $\{10\bar{1}n\}$ CTBs and GTBs from the first-principles, to gain important insights into the formation mechanism of GTBs and also its profound correlation with basal partial dislocations/SFs, TDs, and twin growth.

## 2 Methods

Experimental samples with dimensions of 40 mm × 10 mm × 3 mm were cut from a commercially pure Ti plate, annealed in vacuum at 650 °C for 1 h, and then cold-rolled to 40% thickness reduction. TEM specimens were then cut from the transverse section of the rolled sheets and ground to 50 μm in thickness. The HRTEM characterization was performed using a FEI Titan G2 60−300 TEM with an image spherical aberation corrector operated at 300 kV.

All the DFT calculations were conducted using Vienna ab-initio simulation package (VASP) [37] with the plane-wave basis sets and periodic boundary conditions. The electron-core interaction was described by the Blöchl projector augmented wave method (PAW) within the frozen-core approximation [38]. The Perdew−Burke−Ernzerhof (PBE) generalized gradient approximation was employed for exchange-correlation functions [39]. Sandwich supercell models were employed to calculate the $\{10\bar{1}1\}$, $\{10\bar{1}2\}$ and $\{10\bar{1}3\}$ TB interfaces. All the ground-state configurations were optimized using a high energy cutoff of 475 eV for the plane-wave basis sets until the total energy was minimized and the total force on each ion converged within 0.02 eV/Å.

## 3 Results and discussion

### 3.1 Basic structures and energetics

Figure 1(a) schematically illustrates the major twinning modes in hcp Ti lattice. Figures 1(b−d) show the projections of the corresponding CTBs along $\boldsymbol{a}_1=\langle\bar{1}2\bar{1}0\rangle$. Hollow and solid balls denote atoms on two different neighboring $\{1\bar{1}00\}$ planes. Dashed lines represent $\{0001\}$ planes with an -ABABAB- stacking sequence, and solid frames highlight the conventional unit cells as viewed along $\boldsymbol{a}_1$. Interface formation energy ($\gamma_{\mathrm{CTB}}$) was then calculated as

$$\gamma_{\mathrm{CTB}}=\frac{1}{2A}(E_{\mathrm{CTB}}-E_{\mathrm{bulk}}) \quad (1)$$

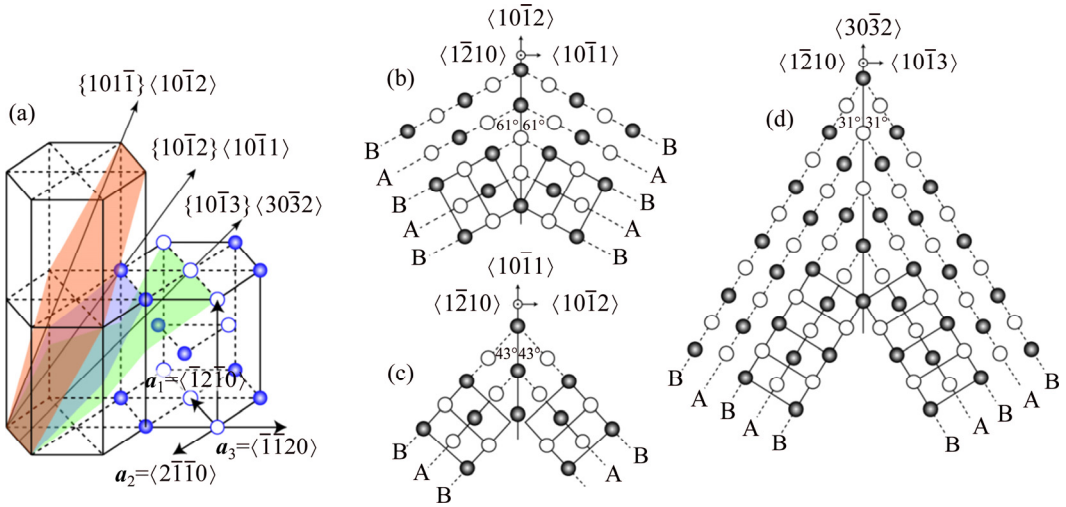


**Fig. 1** Schematics for {10$\bar{1}$1}⟨10$\bar{1}$2⟩, {10$\bar{1}$2}⟨10$\bar{1}$1⟩, and {10$\bar{1}$3}⟨30$\bar{3}$2⟩ twinning modes in hcp Ti (a) and ⟨1$\bar{2}$10⟩ projections of {10$\bar{1}$1}, {10$\bar{1}$2}, and {10$\bar{1}$3} CTBs (b−d)

where $E_{CTB}$ and $E_{bulk}$ are the total energy of a fully relaxed CTB supercell and a pure bulk supercell with the exact same number of atoms, respectively, and $A$ is the boundary area. The {10$\bar{1}$1}, {10$\bar{1}$2}, and {10$\bar{1}$3} CTB supercells contain 64, 88, and 64 Ti atoms with periodic boundary conditions, respectively. Each supercell hosted two identical twin boundaries with a separation of at least 10 Å. Their dimensions along ⟨1$\bar{2}$10⟩ are all equal to the unit lattice parameter $a$. The other dimension along ⟨10$\bar{1}$2⟩, ⟨10$\bar{1}$1⟩, or ⟨30$\bar{3}$2⟩ was chosen to equal $\sqrt{3a^2+4c^2}$, $\sqrt{12a^2+4c^2}$, or $\sqrt{27a^2+4c^2}$ for {10$\bar{1}$1}, {10$\bar{1}$2}, or {10$\bar{1}$3} CTBs, respectively, to sufficiently cover one stacking period and retain the inversion symmetry. Accordingly, the Brillouin-zone integrations employed a 4×13×1, 4×8×1, and 2×15×2 $\Gamma$-centered Monkhorst−Pack K-mesh, respectively. Each supercell hosted two identical twin boundaries with a separation distance of more than 10 Å, to minimize the possible interaction. The calculated results are summarized in Table 1,

**Table 1** Calculated interface energies of {10$\bar{1}n$} CTBs in hcp Ti

| CTB type | $\gamma_{CTB}$/(J·m$^{-2}$) | |
|---|---|---|
| | This work | Others |
| {10$\bar{1}$1} | 0.090 | DFT: 0.107 [40], 0.075 [21]<br>MD: 0.184 [37], 0.280 [37] |
| {10$\bar{1}$2} | 0.302 | DFT: 0.307 [28], 0.298 [21]<br>MD: 0.273 [28] |
| {10$\bar{1}$3} | 0.343 | DFT: 0.327 [21] |

showing good agreement with all previous DFT calculations. The {10$\bar{1}$1}⟨10$\bar{1}$2⟩ CTB has the lowest formation energy of 0.09 J/m$^2$ only. The {10$\bar{1}$2}⟨10$\bar{1}$1⟩ and {10$\bar{1}$3}⟨30$\bar{3}$2⟩ CTBs require higher formation energies but still lower than those of many symmetric-tilt grain boundaries (normally in the order of ~1 J/m$^2$).

Recall that GTBs can be constructed by gliding along the CTBs. Figure 2(a) shows the supercell for modeling {10$\bar{1}$1} CTB in hcp Ti. Gliding the left half lattice by $b$=1/2⟨10$\bar{1}$2⟩ leads to a high energy and metastable {10$\bar{1}$1} GTB in Fig. 2(b). After a full relaxation, the high energy {10$\bar{1}$1} GTB can transform favorably back into the original CTB structure (with the lowest formation energy of $\gamma$=0.09 J/m$^2$ only), accompanying with a left-shift of the twin boundary (Fig. 2(c)). Once such a gliding-and-shifting process occurs continuously, the {10$\bar{1}$1} CTB can move consistently to the left. An opposite gliding of the left half lattice by −1/2⟨10$\bar{1}$2⟩, however, cannot restore the original {10$\bar{1}$1} CTB structure but can result in a new and high energy structure of $\gamma$=0.635 J/m$^2$. Opposite gliding of the left half lattice of a {10$\bar{1}$2} CTB by $b$=±1/2⟨10$\bar{1}$1⟩ can also fully restore the original {10$\bar{1}$2} CTB structure after relaxation, accompanying with a left-shift of the twin boundary. The {10$\bar{1}$3} CTB is similar with the {10$\bar{1}$1} case: only the 1/2⟨30$\bar{3}$2⟩ gliding can restore the {10$\bar{1}$3} CTB structure with a left-shift of the twin boundary.

We have manifested that all the {10$\bar{1}n$} GTBs are high energy, metastable structures

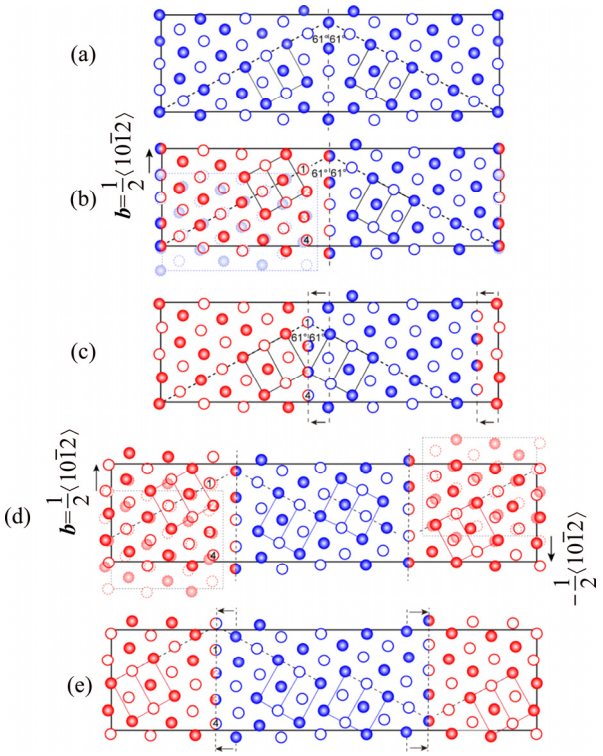


**Fig. 2** Supercell model for $\{10\bar{1}1\}$ CTB in hcp Ti (a), $\{10\bar{1}1\}$ GTB (b) resulted from gliding of $b=1/2\langle 10\bar{1}2\rangle$ from (a), restored $\{10\bar{1}1\}$ CTB (c) after full relaxation of (b), accompanied with left-shift of twin boundary, pair of $\{10\bar{1}1\}$ GTBs (d) resulted from gliding on both sides of twin, and resulted widening of $\{10\bar{1}1\}$ CTB (e) after full relaxation of (d)

compared to their CTB counterparts. It is easy to deduce that simultaneous operation of opposite gliding on both sides of a $\{10\bar{1}n\}$ twin may cause a direct widening of the twin. This has been also manifested by calculations for a $\{10\bar{1}1\}$ twin supercell (Figs. 2(d) and (e)) employing 80 Ti atoms and a 4×10×1 $\Gamma$-centered Monkhorst−Pack K-mesh for Brillouin-zone integration. A twin growth mechanism can be thus suggested as the continuous opposite gliding on both sides of the twin. We notice that the above gliding twin modes of $\{10\bar{1}1\}\langle 10\bar{1}2\rangle$, $\{10\bar{1}2\}\langle 10\bar{1}1\rangle$, and $\{10\bar{1}3\}\langle 30\bar{3}2\rangle$ are not among common slip systems in hcp Ti, and one may thus expect that such gliding could be hardly induced by shear strains in real practice.

### 3.2 Roles of basal stacking faults (SFs)

Considering the important role of SFs in twin growth in cubic metals [41,42] and the relatively low formation energy of basal SFs in hcp Ti (~0.150 J/m$^2$ for SF-$I_1$, 0.260−0.350 J/m$^2$ for SF-$I_2$, ~0.360 J/m$^2$ for SF-$E$ [43,44]), we turned to explore the implications of basal SFs on GTB formation and the subsequent twin growth in hcp Ti. A basal edge dislocation with a unit Burgers vector can dissociate into two Shockley partial dislocations as $1/3\langle 11\bar{2}0\rangle=1/3\langle 10\bar{1}0\rangle+1/3\langle 01\bar{1}0\rangle$ [45] (see Fig. 3(a)). Three basic types of basal SFs can result in Fig. 3(b): (1) extrinsic SF-$E$, having a stacking sequence of -(ABABCABAB)-, formed by inserting an extra basal plane, (2) intrinsic SF-$I_2$, having a stacking sequence of -(ABABCACA)-, formed from a slip of $1/3\langle 01\bar{1}0\rangle$, and (3) intrinsic SF-$I_1$, having a stacking sequence of -(ABABCBCB)-, formed by removing one basal layer followed by a slip of $1/3\langle 01\bar{1}0\rangle$. Using a $\{10\bar{1}1\}$ twin as an illustrative example, the $\langle\bar{1}2\bar{1}0\rangle$ projections of these basal SFs and SF-impacted TBs are shown in Figs. 3(c−e). Introducing either an SF-$E$ or an SF-$I_2$ to the left side lattice (see Fig. 3(c) or (d)) led to a high energy TB structure after relaxation, while the TB with an SF-$I_1$ in Fig. 3(e) reproduced exactly the $\{10\bar{1}1\}$ GTB structure of Fig. 2(b). This GTB can then favorably relax into the original, low energy CTB structure, accompanying with moving of the boundary (see Fig. 2). Such a structural correlation between SF-$I_1$ and CTB was also predicted for $\{10\bar{1}2\}$ and $\{10\bar{1}3\}$ twins, which strongly suggests that SF-$I_1$ could induce the gliding, to initiate twin widening and growth. Recall that the formation of SF-$I_1$ involves partial dislocations on basal slip planes (see Fig. 3(b)). We can thus deduce that, on $\{10\bar{1}n\}$ twin planes, by inducing basal SF-$I_1$ (Fig. 3(b)), basal partial dislocations may cause the TB gliding in favor of the widening and growth of $\{10\bar{1}n\}$ twins.

### 3.3 Twinning disconnections (TDs)

Figure 4 schematically reviews how basal SF-$I_1$ can induce twin widening and growth. When basal SFs (SF-$I_1$) reach a $\{10\bar{1}1\}$ twin from both sides, high energy GTB segments form in Fig. 4(b). Each segment relaxes back to a low energy CTB structure, causing the TB gliding and also leaving behind a pair of single-layer TDs. Clearly, the distance between $I_1$ SFs determines the initial separation distance of the TD pairs, and the twin thus becomes serrated with TD steps in Fig. 4(c). Please note that this kind of TD steps have been

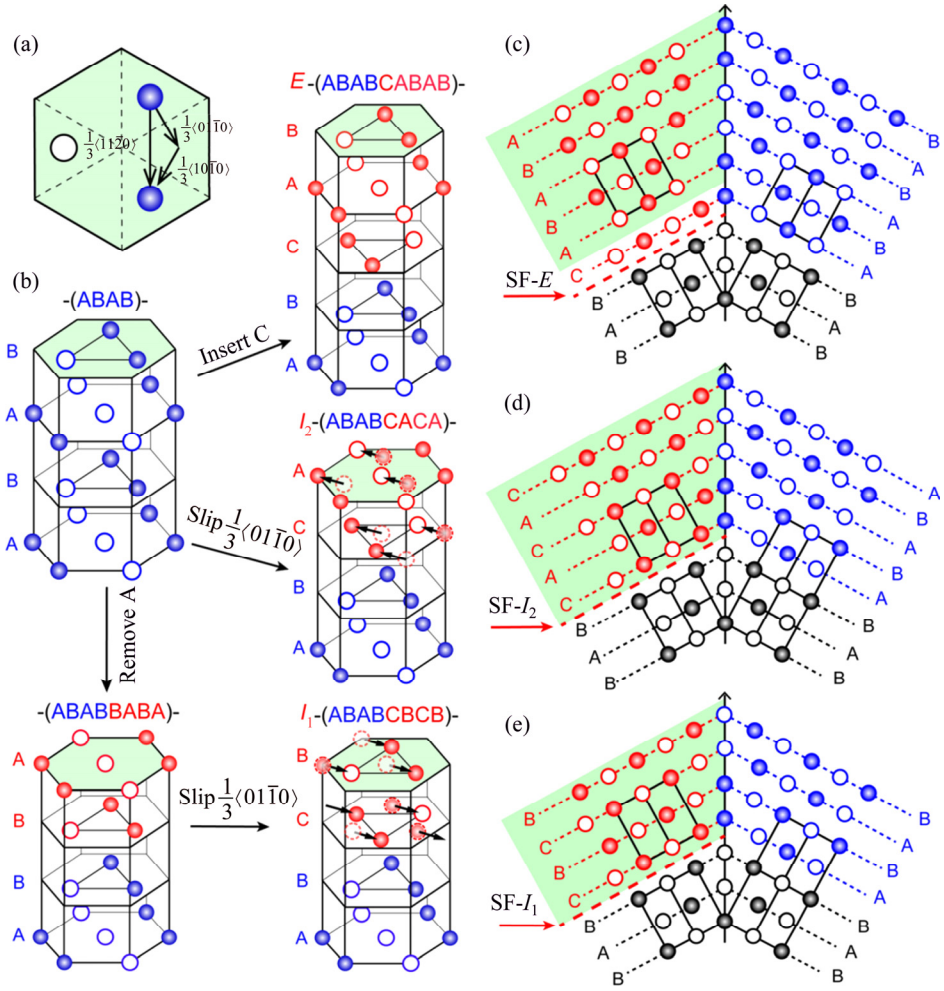


**Fig. 3** Schematic for basal edge dislocation dissociation into two Shockley partials (a), formation of basal SFs $I_1$, $I_2$, and $E$ (b), SF-$E$ (c), SF-$I_2$ (d), and SF-$I_1$ (e) impacted $\{10\bar{1}1\}$ CTBs (Blue atoms represent perfect matrix lattice, and black atoms represent SF-free segment of $\{10\bar{1}1\}$ CTB)

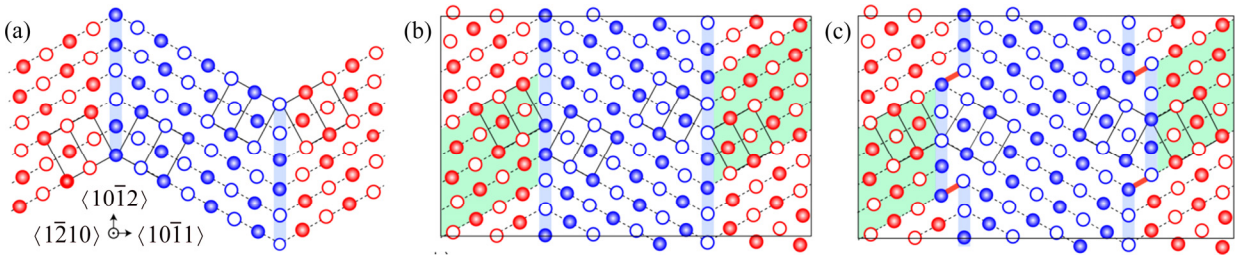


**Fig. 4** $\{10\bar{1}1\}$ twin embedded in hcp Ti matrix (a), supercell model for $\{10\bar{1}1\}$ twin with SF-$I_1$ generated on both sides (b) and formation of TDs and twin widening (c) induced by SF-$I_1$ after full relaxation from (b) (Green shadows highlight SF-$I_1$ regions and red bars locate single-layer TD steps)

observed very recently in Mg and its roles on twin boundary mobility have also been suggested [46]. Also, the single-layer TDs in Fig. 4(c) can be labelled as $\{0001\}_{\text{matrix}}//\{10\bar{1}1\}_{\text{twin}}$ basal-pyramidal (BPy) steps, where the basal plane $\{0001\}$ of the matrix (the red lattice) is exactly parallel to the pyramidal plane $\{10\bar{1}1\}$ of the twin (the blue lattice). It can be naturally deduced that an accumulation of basal SFs could induce the pileup of TDs, leading to the formation of multiple wide BPy steps at the twin boundary. This has been confirmed in our pure Ti samples using HRTEM, as observed for $\{10\bar{1}1\}$ twins under the zone axis of $[1\bar{2}10]_{\text{hcp}}$ in Fig. 5. The coherent $\{10\bar{1}1\}$ twin boundaries and multiple wide BPy steps are marked using yellow and red dashed lines, respectively.

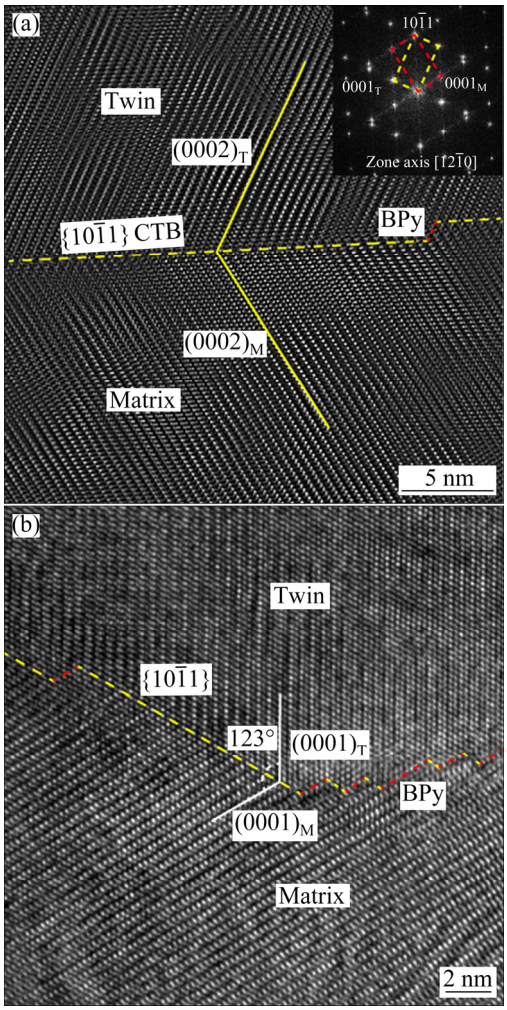


**Fig. 5** HRTEM images of $\{10\bar{1}1\}$ CTB with single, two-layer TD, or basal-pyramidal (BPy) step (Twin orientation relation was verified by the inserted Fast Fourier Transformation (FFT) pattern) (a) and serrated $\{10\bar{1}1\}$ CTB featured with multiple, wider BPy steps (b)

The formation energy of TD can be further predicted as

$$\gamma_{TD}=[E_{CTB+TD}-(\gamma_{CTB}A_{CTB}+\gamma_{SF}A_{SF}+n\mu_{Ti})]/(mA_{TD}) \quad (2)$$

where $E_{CTB+TD}$ is the total energy of the supercell in Fig. 4(c); $\gamma_{CTB}$ is the interface formation energy of the CTB as calculated using Eq. (1); $\gamma_{SF}$ is the energy of SF per unit area, using 0.150 J/m$^2$ [40,41]; $A_{CTB}$, $A_{SF}$, and $A_{TD}$ are the areas of the CTB, the SF, and the TD step, respectively; $\mu_{Ti}$ is the chemical potential of Ti in its pure bulk; $m$ is the total number of TDs in the supercell, i.e. $m$=4; $n$ is the total number of Ti atoms in the supercell. The $\{10\bar{1}1\}$ twin supercell in Fig. 4(c) employed 128 Ti atoms, i.e. $n$=128. Brillouin-zone integration employed an 1×7×1 $\Gamma$-centered Monkhorst−Pack K-mesh. Using Eq. (2), the formation energy of the TD step was predicted to be 0.572 J/m$^2$, much higher than that of the $\{10\bar{1}1\}$ CTB. This is simply due to the incoherent boundary feature of the TD (or BPy) steps as clearly seen in Fig. 4(c) and Fig. 5.

### 3.4 Pinning effect of segregated solutes

In Ti-based alloys, the formation of TDs through the SF-$I_1$ induced gliding could be affected by alloying solutes. We further evaluated the pinning effect of segregated solutes on the gliding of a $\{10\bar{1}1\}$ CTB by calculating the corresponding energy change as

$$\Delta E_b(x)=E^x_{GTB}-E^x_{CTB} \quad (3)$$

where $E^x_{CTB}$ and $E^x_{GTB}$ are the total energies of single solute $x$ segregated CTB before and after the gliding, respectively. As the direct consequence of gliding, the CTB involves into its GTB counterpart that has a high energy and metastable structure. Various solutes that are commonly added into Ti alloys have been considered, including $\alpha$-Ti stabilized solutes Al and Ge, $\beta$-Ti stabilized solutes Ag and V, and neutral solutes Y and Zr. Figure 6 shows possible segregation sites (sites 1−6) on the CTB plane and its neighbourhood. It should be noted that the relaxed structures and the

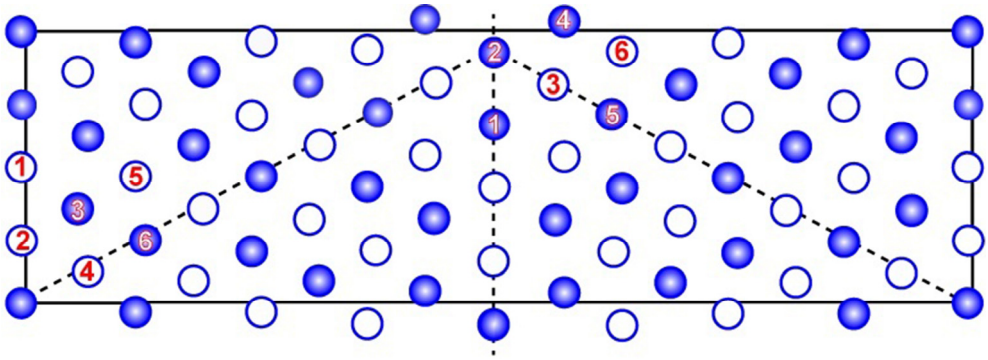


**Fig. 6** Possible sites for solute segregation on $\{10\bar{1}1\}$ CTB plane or its first or second neighboring plane

**Table 2** Calculated energy change $\Delta E_b$ for gliding of $\{10\bar{1}1\}$ CTB with different segregation concentrations

| Solute concentration/% | $\Delta E_b$/eV | | | | | | |
|---|---|---|---|---|---|---|---|
| | Pure Ti | Y (Site 1) | Zr (Site 1) | Al (Site 2) | Ge (Site 2) | Ag (Site 1) | V (Site 2) |
| 3.12 | 1.153 | 1.491 | 1.269 | 1.226 | 1.606 | 1.673 | 1.407 |
| 6.24 | 1.153 | 1.493 | 1.325 | 1.313 | 2.155 | 2.112 | 1.659 |

corresponding total energies of the CTB and GTB are exactly identical. For all these solutes considered, the most favoured segregation site was found always to be Site 1 or Site 2 right on the CTB plane, corresponding to a segregation concentration of ~3.12%. Please note that Site 1 or Site 2 has one equivalent site within one stacking period along the CTB plane. Thus, using the supercell in Fig. 6, we can consider a higher segregation concentration of ~6.24%. The calculated $\Delta E_b$ results under the two segregation concentrations are compared in Table 2.

Higher positive $\Delta E_b$ values predict larger energy barriers for the twin gliding. It can be thus suggested from Table 2 that all the considered solute elements have a pinning effect on the $\{10\bar{1}1\}$ CTB gliding as compared to pure Ti. Among which, Zr and Al have relatively small influence. Ag and Ge show a fairly strong capability for pinning the twin boundary, followed by Y and V. Increasing the segregation concentration always enhances the pinning effect to different extents, but this trend is not obvious for Y. The solute pinning effect can certainly benefit in strengthening the matrix by stabilizing twin sizes [46,47]. In this regard, these phase-stabilizing solute elements in Ti could be re-classified into three different categories: strong twin-stabilizing solutes Ag and Ge, medium-strong twin-stabilizing solutes Y and V, and weak twin-stabilizing solutes Zr and Al. Our predicted pinning effects of various solutes on twin boundaries in Ti alloys await future experimental validation.

## 4 Conclusions

(1) $\{10\bar{1}n\}$ GTBs are metastable structures compared to their CTB counterparts and can be resulted from the gliding of CTBs. The simultaneous operation of opposite gliding on both sides of a twin may cause the twin widening. A new twin growth mechanism can be suggested through the continuous opposite gliding on both sides of the twin when subjected to shear strain.

(2) Another new twin growth mechanism can be also suggested based on the CTB interaction with intrinsic basal SF-$I_1$. Basal SFs can induce the gliding of CTBs, and further the formation and pileup of TDs on the CTB plane as observed in HRTEM, which can facilitate the twin widening and growth.

(3) Furthermore, solute segregation can also favourably affect the TB gliding. New strengthening strategies can be thus suggested for Ti alloys by direct pinning twin boundaries using strong twin-stabilizing solute elements, such as Ag and Ge.

## Acknowledgments

The authors would like to thank the financial support from the National MCF Energy R & D Program of China (2018YFE0306100), the National Natural Science Foundation of China (51971249) and the State Key Laboratory for Powder Metallurgy, Central South University, Changsha, China. The computational resource at the High Performance Computing Center of Central South University is also gratefully acknowledged.

## References

[1] GONG M Y, HIRTH J P, LIU Y, SHEN Y, WANG J. Interface structures and twinning mechanisms of $\{\bar{1}012\}$ twins in hexagonal metals [J]. Materials Research Letters, 2017, 5(7): 449−464.

[2] WANG Y M, SANSOZ F, LAGRANGE T, OTT R T, MARIAN J, BARBEE T W Jr, HAMZA A V. Defective twin boundaries in nanotwinned metals [J]. Nature Materials, 2013, 12(8): 697−702.

[3] WANG J W, CAI X B, SHI R, WU Z F, WANG W J, LONG G, TANG Y J, CAI N D, OUYANG W K, GENG P, CHANDRASHEKAR B N, AMINI A, WANG N, CHENG C. Twin defect derived growth of atomically thin $MoS_2$ dendrites [J]. ACS Nano, 2018, 12(1): 635−643.

[4] FULLMAN R L, FISHER J C. Formation of annealing twins during grain growth [J]. Journal of Applied Physics, 1951, 22(11): 1350−1355.

[5] HUANG C X, WANG K, WU S D, ZHANG Z F, LI G Y, LI S. Deformation twinning in polycrystalline copper at room temperature and low strain rate [J]. Acta Materialia, 2006, 54(3): 655−665.

[6] HIRTH J P, WANG J, TOME C N. Disconnections and other defects associated with twin interfaces [J]. Progress in Materials Science, 2016, 83: 417−471.

[7] CHRISTIAN J W, MAHAJAN S. Deformation twinning [J]. Progress in Materials Science, 1995, 39(1−2): 1−157.

[8] AVEDESIAN M M, BAKER H. Magnesium and magnesium alloys [M]. Ohio: Materials Park, 1999.

[9] HIRTH J P, POND R C. Steps, dislocations and disconnections as interface defects relating to structure and phase transformations [J]. Acta Materialia, 1996, 44(12): 4749−4763.

[10] WANG J, LIU L, TOME C N, MAO S X, GONG S K. Twinning and de-twinning via glide and climb of twinning dislocations along serrated coherent twin boundaries in hexagonal-close-packed metals [J]. Materials Research Letters, 2013, 1(2): 81−88.

[11] WANG J, BEYERLEIN I J, HIRTH J P, TOMÉ C N. Twinning dislocations on $\{\bar{1}011\}$ and $\{\bar{1}013\}$ planes in hexagonal close-packed crystals [J]. Acta Materialia, 2011, 59(10): 3990−4001.

[12] WANG J, HIRTH J P, TOMÉ C N. $(\bar{1}012)$ twinning nucleation mechanisms in hexagonal-close-packed crystals [J]. Acta Materialia, 2009, 57(18): 5521−5530.

[13] THOMPSON N, MILLARD D J. XXXVIII. Twin formation, in cadmium [J]. Philosophical Magazine, 2010, 43(339): 422−440.

[14] SERRA A, BACON D J. A new model for $\{10\bar{1}2\}$ twin growth in hcp metals [J]. Philosophical Magazine A, 2006, 73(2): 333−343.

[15] MENDELSON S. Zonal dislocations and twin lamellae in h.c.p. metals [J]. Materials Science and Engineering, 1969, 4(4): 231−242.

[16] SERRA A, BACON D J. On the generation of twinning dislocations in hcp twin boundaries [J]. Materials Science Forum, 1996, 207: 553−556.

[17] BRAISAZ T. High-resolution electron microscopy study of the $(10\bar{1}2)$ twin and defects analysis in deformed polycrystalline alpha titanium [J]. Philosophical Magazine Letters, 2010, 74(5): 331−338.

[18] BRAISAZ T, RUTERANA P, NOUET G. Twin tip defects related to the nucleation and growth mechanisms of the twin $(10\bar{1}2)$ in zinc characterized by high-resolution electron microscopy [J]. Philosophical Magazine A, 1997, 76(1): 63−84.

[19] LI B, MA E. Atomic shuffling dominated mechanism for deformation twinning in magnesium [J]. Physical Review Letters, 2009, 103(3): 035503.

[20] LI B, MA E. Zonal dislocations mediating $\{10\bar{1}1\}\langle 10\bar{1}\bar{2}\rangle$ twinning in magnesium [J]. Acta Materialia, 2009, 57(6): 1734−1743.

[21] KUMAR A, WANG J, TOME C N. First-principles study of energy and atomic solubility of twinning-associated boundaries in hexagonal metals [J]. Acta Materialia, 2015, 85: 144−154.

[22] BHATIA M A, SOLANKI K N. Energetics of vacancy segregation to symmetric tilt grain boundaries in hexagonal closed pack materials [J]. Journal of Applied Physics, 2013, 114(24): 244309.

[23] WANG J, BEYERLEIN I J. Atomic structures of symmetric tilt grain boundaries in hexagonal close packed (hcp) crystals [J]. Modelling and Simulation in Materials Science and Engineering, 2012, 20(2): 024002.

[24] ZHANG J, DOU Y C, ZHENG Y. Twin-boundary segregation energies and solute-diffusion activation enthalpies in Mg-based binary systems: A first-principles study [J]. Scripta Materialia, 2014, 80: 17−20.

[25] TSURU T, SOMEKAWA H, CHRZAN D C. Interfacial segregation and fracture in Mg-based binary alloys: Experimental and first-principles perspective [J]. Acta Materialia, 2018, 151: 78−86.

[26] HAGÈGE S, MORI M, ISHIDA Y. Computer simulation of the $(10\bar{1}2)$ twin atomic structure in HCP metals [J]. Le Journal de Physique Colloques, 1990, 51(C1): C1-161−C1-166.

[27] BRAISAZ T, RUTERANA P, LEBOUVIER B, NOUET G. Atomic structure analysis of the $(10\bar{1}2)$ twin in zinc by HREM and energetical calculations [J]. Physica Status Solidi B—Basic Solid State Physics, 1995, 191(2): 267−281.

[28] MORRIS J R, YE Y Y, YOO M H. First-principles examination of the $(10\bar{1}2)$ twin boundary in hcp metals [J]. Philosophical Magazine, 2005, 85(2−3): 233−238.

[29] WANG Y, CHEN L Q, LIU Z K, MATHAUDHU S N. First-principles calculations of twin-boundary and stacking-fault energies in magnesium [J]. Scripta Materialia, 2010, 62(9): 646−649.

[30] PEI Z R, ZHANG X, HICKEL T, FRIAK M, SANDLOBES S, DUTTA B, NEUGEBAUER J. Atomic structures of twin boundaries in hexagonal close-packed metallic crystals with particular focus on Mg [J]. NPJ Computational Materials, 2017, 3(1): 6.

[31] WANG C, WANG H Y, HUANG T L, XUE X N, QIU F, JIANG Q C. Generalized-stacking-fault energy and twin-boundary energy of hexagonal close-packed Au: A first-principles calculation [J]. Scientific Reports, 2015, 5: 10213.

[32] HIRTH J P, LOTHE J, MURA T. Theory of dislocations [J]. Journal of Applied Mechanics, 1983, 50: 476−477.

[33] ZHANG X Y, LI B, LIU Q. Non-equilibrium basal stacking faults in hexagonal close-packed metals [J]. Acta Materialia, 2015, 90: 140−150.

[34] WANG F, BARRETT C D, MCCABE R J, EL KADIRI H, CAPOLUNGO L, AGNEW S R. Dislocation induced twin growth and formation of basal stacking faults in $\{10\bar{1}2\}$ twins in pure Mg [J]. Acta Materialia, 2019, 165: 471−485.

[35] OSTAPOVETS A, SERRA A, POND R C. Non-diffusional growth mechanism of $I_1$ basal stacking-faults inside twins in hcp metals [J]. Scripta Materialia, 2019, 172: 149−153.

[36] OSTAPOVETS A, SERRA A. Slip dislocation and twin nucleation mechanisms in hcp metals [J]. Journal of Materials Science, 2016, 52(1): 533−540.

[37] KRESSE G, FURTHMÜLLER J. Efficiency of ab-initio total energy calculations for metals and semiconductors using a plane-wave basis set [J]. Computational Materials Science, 1996, 6(1): 15−50.

[38] KRESSE G, JOUBERT D. From ultrasoft pseudopotentials to the projector augmented-wave method [J]. Physical Review B, 1999, 59(3): 1758−1775.

[39] PERDEW J P, BURKE K, EMZEHOF M. Generalized gradient approximation made simple [J]. Physical Review

Letters, 1996, 77(18): 3865−3868.
[40] YOO M H, MORRIS J R, HO K M, AGNEW S R. Nonbasal deformation modes of HCP metals and alloys: Role of dislocation source and mobility [J]. Metallurgical and Materials Transactions A—Physical Metallurgy and Materials Science, 2002, 33(3): 813−822.
[41] MAHAJAN S, CHIN G Y. Formation of deformation twins in f.c.c. crystals [J]. Acta Metallurgica, 1973, 21(10): 1353−1363.
[42] LI S Z, DING X D, DENG J K, LOOKMAN T, LI J, REN X B, SUN J, SAXENA A. Superelasticity in bcc nanowires by a reversible twinning mechanism [J]. Physical Review B, 2010, 82(20): 205435.
[43] BENOIT M, TARRAT N, MORILLO J. Density functional theory investigations of titanium $\gamma$-surfaces and stacking faults [J]. Modelling and Simulation in Materials Science and Engineering, 2013, 21(1): 015009.
[44] TARRAT N, BENOIT M, MORILLO J. Core structure of screw dislocations in hcp Ti: An ab initio DFT study [J]. International Journal of Materials Research, 2009, 100(3): 329−332.
[45] D HULL, BACON D J. Introduction to dislocations [M]. Amsterdam: Elsevier, 2011.
[46] ZHAO X, CHEN H, WILSON N, LIU Q, NIE J F. Direct observation and impact of co-segregated atoms in magnesium having multiple alloying elements [J]. Nature Communications, 2019, 10(1): 3243.
[47] NIE J F, ZHU Y M, LIU J Z, FANG X Y. Periodic segregation of solute atoms in fully coherent twin boundaries [J]. Science, 2013, 340(6135): 957−960.

# 密排六方钛中基面堆垛层错导致的孪晶界滑移、孪生台阶及孪晶生长：第一性原理研究

钱 琦[1*]，刘正卿[1*]，江 勇[1,2]，王怡人[1]，安星龙[2]，宋 旼[2]

1. 中南大学 材料科学与工程学院，长沙 410083；
2. 中南大学 粉末冶金国家重点实验室，长沙 410083

**摘 要：**基于第一性原理计算研究密排六方结构钛中 $\{10\bar{1}n\}$ 共格孪晶界和滑移孪晶界的结构和能量，探讨滑移孪晶界的形成机理及其与孪晶生长的关系。结果表明，共格孪晶界与基面堆垛层错的相互作用可使共格孪晶界产生滑移，从而形成对应的滑移孪晶界。这种滑移最终能在孪晶界处形成一对单层孪生台阶，并恢复共格孪晶界的结构。孪生台阶的塞积可导致高分辨率透射电镜观察到的孪晶界上的台阶宽化，进一步促进孪晶的生长。此外，还评估多种合金化元素对孪晶界滑移的钉扎效应，为钛合金的强化设计提供指导。

**关键词：**孪晶界；层错；孪生台阶；孪晶生长；第一性原理

**(Edited by Wei-ping CHEN)**